

# CALIBRATION ERRORS IN INTERFEROMETRIC RADIO POLARIMETRY

CHRISTOPHER A. HALES<sup>1, 2, \*</sup>

<sup>1</sup>*National Radio Astronomy Observatory, PO Box 0, Socorro, NM 87801, USA*

<sup>2</sup>*School of Mathematics and Statistics, Newcastle University, Newcastle upon Tyne NE1 7RU, UK*

## ABSTRACT

Residual calibration errors are difficult to predict in interferometric radio polarimetry because they depend on the employed observational calibration strategy, encompassing the Stokes vector of the calibrator and parallactic angle coverage. This work presents analytic derivations and simulations that enable examination of residual on-axis instrumental leakage and position angle errors for a suite of calibration strategies. The focus is on arrays comprising alt-az antennas with common feeds over which parallactic angle is approximately uniform. The results indicate that calibration schemes requiring parallactic angle coverage in the linear feed basis (e.g. ALMA) need only observe over  $30^\circ$ , beyond which no significant improvements in calibration accuracy are obtained. In the circular feed basis (e.g. VLA above 1 GHz),  $30^\circ$  is also appropriate when the Stokes vector of the leakage calibrator is known a priori, but this rises to  $90^\circ$  when the Stokes vector is unknown. These findings illustrate and quantify concepts that were previously obscure rules of thumb.

*Keywords:* methods: analytical — methods: data analysis — methods: observational  
 — techniques: interferometric — techniques: polarimetric

## 1. INTRODUCTION

The mathematical foundations of interferometric radio polarimetry were first formulated two decades ago by Hamaker et al. (1996). Their work marked a significant improvement over the previous ‘black box’ approach presented by Morris et al. (1964) (see also Gardner & Whiteoak 1966 for an early history of radio polarimetry). The formalism developed by Hamaker et al. (1996) continues to underpin cutting edge developments in calibration (e.g. Smirnov 2011).

In a companion paper, Sault et al. (1996) examined the practicalities of calibrating an array in the presence of errors due to incorrect assumptions about calibrators or poorly determined parameters in the calibration process. An insightful summary of the manner in which these various influences will lead to corruption of calibration parameters was presented in Table 1 of Sault et al. (1996). However, it is not trivial to convert between the parameters presented in this seminal work and the errors implied for calibrated data because this requires taking into account the employed observational calibration strategy. An accessible overview of these errors is needed to design efficient observing schemes in the present era of increasing telescope automation. It is also needed more generally as an educational tool to foster deeper understanding of radio polarimetry.

Some efforts have been made to improve this situation, such as the investigation of dynamic range limitations presented by Sault & Perley (2014). However, other fundamental questions remain unaddressed. For example, what is the fractional polarization below which a calibrator can be assumed to be unpolarized, or the requirements on a calibrator’s minimum coverage in parallactic angle<sup>1</sup> throughout synthesis, to ensure that post-calibration residual instrumental polarization or position angle errors remain below nominated thresholds.

The aim of this work is to fill the gap by presenting a practical guide to errors in interferometric radio polarimetry that explicitly accounts for calibration strategy. The structure is as follows. Section 2 presents general assumptions concerning the types of interferometric arrays and the observational parameter space that will be considered in this work. Section 3 presents a concise overview of polarization fundamentals, providing conceptual and notational context for the remaining work. Section 4 explores calibration strategies involving unpolarized and polarized calibrators, examining the roles that a calibrator’s fractional polarization, signal to noise, and parallactic angle coverage play in limiting post-calibration residual instrumental polarization. The same parameter space is explored in Section 5 but with a focus on position angle errors. Section 6 concludes.

## 2. ASSUMPTIONS

This work will assume an interferometric array with the following characteristics. First, all feeds are alt-az mounted, i.e. situated on alt-az antennas without dish rotators such as those used on the Australian Square Kilometre Array Pathfinder (ASKAP). Second, there are at least 3 baselines; closure between  $N \geq 3$  antennas is required to solve for of order  $N$  matrices from  $N(N-1)/2$  baselines (Sault et al. 1996). Third, parallactic angle ( $\psi$ ) is constant across the array, within mechanical alignment errors, such that  $\psi_i = \psi$  for all  $i$  antennas (i.e. the array is small). And fourth, all antennas are fitted with dual orthogonal linear (X, Y) or circular (R, L) feeds with the same nominal alignment, forming a homogeneous array. From these, all polarization products are measured.

<sup>1</sup> Parallactic angle is that constructed at a celestial coordinate between a line of constant right ascension and one pointing toward zenith, as viewed from a geographic coordinate. It describes the orientation of the sky as it rotates within the field of view of an alt-az telescope. To illustrate, see <https://github.com/chrishales/plotparang> for publicly available code to plot parallactic angle coverage while accounting for telescope elevation limits.

Polarization calibrators will be assumed unresolved and located on-axis. The off-axis polarimetric response of the system will not be considered. Any frequency dependence of parameters will be assumed implicitly.

This work will focus on linear polarimetry<sup>2</sup>. Circular polarization calibration will be touched on for completeness in Section 3, but no error analysis will be pursued (where circular to linear leakage effects, or vice versa, may be important).

Results will be illustrated for two representative arrays: the Atacama Large Millimeter/submillimeter Array (ALMA) which observes with linear feeds in all bands, and the Karl G. Jansky Very Large Array (VLA) which observes with circular feeds in all bands above 1 GHz.

Terminology and notation throughout this work will follow conventions from the widely used Common Astronomy Software Applications package (CASA; McMullin et al. 2007).

### 3. POLARIZATION FUNDAMENTALS

The radio interferometer measurement equation (Hamaker et al. 1996; Sault et al. 1996; Noordam 1996; Smirnov 2011) relates observed visibilities to ideal model visibilities on a baseline between antennas  $i$  and  $j$  as

$$\mathbf{V}_{ij}^{obs} = \mathbf{B}_{ij} \mathbf{G}_{ij} \mathbf{D}_{ij} \mathbf{P}_{ij} \mathbf{V}_{ij}^{mod} \quad (1)$$

where the corrupting Mueller matrix terms (frequency-dependent outer products of antenna-based Jones matrices;  $\mathbf{M}_{ij} = \mathbf{J}_i \otimes \mathbf{J}_j^*$ ) are associated from right to left with parallactic angle, instrumental polarization leakage, combined electronic and atmospheric gains, and bandpass, respectively. Some terms are neglected above for clarity (e.g. Faraday rotation and phase delay associated with the ionosphere/plasmasphere, antenna elevation-dependence, non antenna-based terms). Calibration involves solving for these terms and applying their inverse to the observed data to recover corrected data

$$\mathbf{V}^{corr} = \mathbf{P}^{-1} \mathbf{D}^{-1} \mathbf{G}^{-1} \mathbf{B}^{-1} \mathbf{V}^{obs} \quad (2)$$

where antenna indices will now be omitted unless required for clarity. While the corrupting terms in the measurement equation are written as independent effects along the signal path (i.e. from right to left in Equation 1), in general they are not. Care must therefore be taken to distinguish dominant terms from those that are coupled to others. The former can be solved for independently, while the latter require an iterative approach to converge on a global solution over multiple terms<sup>3</sup>.

The measurement equation is typically refactored to the relative phase frame of the bandpass/gain reference antenna (phase fixed to zero in both polarizations on this antenna)

$$\mathbf{V}^{obs} = \mathbf{B}_r \mathbf{G}_r \mathbf{K}_{crs} \mathbf{D}_r \tilde{\mathbf{X}}_r \mathbf{P} \mathbf{V}^{mod} \quad (3)$$

in which the refactored terms are identified by subscript  $r$ , the crosshand bandpass phase<sup>4</sup> on the reference antenna  $\mathbf{X}_r$  that arises from the refactoring of  $\mathbf{B} \mathbf{G} = \mathbf{B}_r \mathbf{G}_r \mathbf{X}_r$  remains unconstrained,  $\mathbf{X}_r = \mathbf{K}_{crs} \tilde{\mathbf{X}}_r$  is separated into crosshand delay  $\mathbf{K}_{crs}$  and crosshand phase  $\tilde{\mathbf{X}}_r$  terms that capture first-order linear and residual non-linear frequency dependence, respectively, and leakages  $\mathbf{D}_r = \mathbf{X}_r \mathbf{D} \mathbf{X}_r^{-1}$  are measured in the crosshand phase frame<sup>5</sup>.

<sup>2</sup> Circular, linear, and elliptical polarization will be indicated in this work by  $\mathcal{V}$ ,  $\mathcal{L} = \sqrt{\mathcal{Q}^2 + \mathcal{U}^2}$ , and  $\mathcal{P} = \sqrt{\mathcal{V}^2 + \mathcal{L}^2}$ , respectively, formed from the Stokes parameters  $\mathcal{Q}$ ,  $\mathcal{U}$ , and  $\mathcal{V}$ . Fractional values are divided by Stokes  $\mathcal{I}$ .

<sup>3</sup> To illustrate, see the CASA approach to calibration described at [https://casa.nrao.edu/docs/UserMan/casa\\_cookbook016.html](https://casa.nrao.edu/docs/UserMan/casa_cookbook016.html).

<sup>4</sup> Also known in the literature as the  $XY$  phase,  $RL$  phase, or phase-zero difference.

<sup>5</sup> Note that if polarization calibration will be performed, the same reference antenna must be used for all calibration solutions. If this condition is not met, the crosshand phase frame will be ambiguous and polarization calibration will

The leakage terms (‘dipole’ terms or d-terms) describe imperfections in the polarimetric response of the system and quantify the degree to which each feed is sensitive to an orthogonally polarized signal. The imperfections arise from both telescope geometry (e.g. antenna illumination, feed horn, optics alignment) and electronic hardware (e.g. polarization splitter, hybrid coupler). Notation for leakages in this work will follow the Jones matrix form

$$\mathbf{D}_i = \begin{bmatrix} 1 & d_{pi}(\nu) \\ d_{qi}(\nu) & 1 \end{bmatrix} \quad (4)$$

for antenna  $i$  where  $p$  is given by  $X$  (linear basis) or  $R$  (circular basis),  $d_{pi}$  is the fraction of the  $q$  (orthogonal) polarization sensed by  $p$ , and on-diagonal effects are factored into  $\mathbf{B}$  and  $\mathbf{G}$  (Sault et al. 1996<sup>6</sup>). Frequency dependence ( $\nu$ ) will be assumed implicitly throughout this work and omitted below. Other terms from the measurement equation that are most relevant to this work are parallactic angle in the linear feed (LF) and circular feed (CF) bases and crosshand phase on the reference antenna. These take the respective Jones forms

$$\mathbf{P}_i^{\text{LF}} = \begin{bmatrix} \cos \psi & \sin \psi \\ -\sin \psi & \cos \psi \end{bmatrix} \quad (5)$$

and

$$\mathbf{P}_i^{\text{CF}} = \begin{bmatrix} e^{-i\psi} & 0 \\ 0 & e^{i\psi} \end{bmatrix} \quad (6)$$

where  $\psi$  is parallactic angle, and

$$\mathbf{X}_r = \begin{bmatrix} e^{i\rho} & 0 \\ 0 & 1 \end{bmatrix} \quad (7)$$

where  $\rho$  is crosshand phase.

For an interferometer with dual linearly polarized feeds,  $\mathbf{V}^{\text{mod}}$  is given by the 4-element vector

$$V_{XX} = \mathcal{I} + \mathcal{Q} \quad (8)$$

$$V_{XY} = \mathcal{U} + i\mathcal{V} \quad (9)$$

$$V_{YX} = \mathcal{U} - i\mathcal{V} \quad (10)$$

$$V_{YY} = \mathcal{I} - \mathcal{Q} \quad (11)$$

whereas for circular feeds the vector is

$$V_{RR} = \mathcal{I} + \mathcal{V} \quad (12)$$

$$V_{RL} = \mathcal{Q} + i\mathcal{U} \quad (13)$$

$$V_{LR} = \mathcal{Q} - i\mathcal{U} \quad (14)$$

$$V_{LL} = \mathcal{I} - \mathcal{V} \quad (15)$$

be corrupted. This is not a requirement when calibrating only parallel-hand visibility data, which are insensitive to crosshand phase.

<sup>6</sup> Note that Sault et al. (1996) use a different sign convention for d-terms.

The model visibilities for a single baseline, corrupted by parallactic angle, leakage, and crosshand phase terms ( $\mathbf{X}_r \mathbf{D} \mathbf{P} \mathbf{V}^{mod} = \mathbf{G}^{-1} \mathbf{B}^{-1} \mathbf{V}^{obs}$ ), are given in the linear basis by

$$V_{XX} = (\mathcal{I} + \mathcal{Q}_\psi) + \mathcal{U}_\psi (d_{Xi} + d_{Xj}^*) \quad (16)$$

$$V_{XY} = [(\mathcal{U}_\psi + i\mathcal{V}) + \mathcal{I}(d_{Xi} + d_{Yj}^*) - \mathcal{Q}_\psi(d_{Xi} - d_{Yj}^*)] e^{i\rho} \quad (17)$$

$$V_{YX} = [(\mathcal{U}_\psi - i\mathcal{V}) + \mathcal{I}(d_{Yi} + d_{Xj}^*) + \mathcal{Q}_\psi(d_{Yi} - d_{Xj}^*)] e^{-i\rho} \quad (18)$$

$$V_{YY} = (\mathcal{I} - \mathcal{Q}_\psi) + \mathcal{U}_\psi (d_{Yi} + d_{Yj}^*) \quad (19)$$

where  $\mathcal{Q}_\psi \equiv \mathcal{Q} \cos 2\psi + \mathcal{U} \sin 2\psi$ ,  $\mathcal{U}_\psi \equiv \mathcal{U} \cos 2\psi - \mathcal{Q} \sin 2\psi$ , and terms multiplied by second order leakages (e.g.  $d_{Xi} d_{Xj}^*$ ) are neglected. The visibilities in the circular basis are given by

$$V_{RR} = (\mathcal{I} + \mathcal{V}) + d_{Ri} (\mathcal{Q} - i\mathcal{U}) e^{+i2\psi} + d_{Rj}^* (\mathcal{Q} + i\mathcal{U}) e^{-i2\psi} \quad (20)$$

$$V_{RL} = [(\mathcal{Q} + i\mathcal{U}) e^{-i2\psi} + \mathcal{I}(d_{Ri} + d_{Lj}^*) + \mathcal{V}(d_{Lj}^* - d_{Ri})] e^{i\rho} \quad (21)$$

$$V_{LR} = [(\mathcal{Q} - i\mathcal{U}) e^{+i2\psi} + \mathcal{I}(d_{Li} + d_{Rj}^*) + \mathcal{V}(d_{Li} - d_{Rj}^*)] e^{-i\rho} \quad (22)$$

$$V_{LL} = (\mathcal{I} - \mathcal{V}) + d_{Li} (\mathcal{Q} + i\mathcal{U}) e^{-i2\psi} + d_{Lj}^* (\mathcal{Q} - i\mathcal{U}) e^{+i2\psi} \quad (23)$$

Analysis in this work will be restricted to the linearized equations presented above (first order in d-terms). Furthermore, polarization calibration will be limited to examination of cross hand visibilities only, with the additional assumption that Stokes  $\mathcal{V}$  is zero (unless a non-zero model is available). These simplifications are currently used within CASA and are suitable for the focus on linear polarization in this work (note that the full quadratic approach is used in other packages such as MIRIAD; [Sault et al. 1995](#)).

Crosshand phase calibration can be performed (e.g. in CASA) by taking the average over all baselines for the sum of cross hand visibilities,

$$\langle V_{XY} \rangle + \langle V_{YX}^* \rangle = e^{i\rho} [\mathcal{U}_\psi + \mathcal{I} \langle d_{Xi} + d_{Yi}^* + d_{Xj} + d_{Yj}^* \rangle - \mathcal{Q}_\psi \langle d_{Xi} - d_{Yi}^* + d_{Xj} - d_{Yj}^* \rangle] \quad (24)$$

$$\langle V_{RL} \rangle + \langle V_{LR}^* \rangle = e^{i\rho} [(\mathcal{Q} + i\mathcal{U}) e^{-i2\psi} + \mathcal{I} \langle d_{Ri} + d_{Li}^* + d_{Rj} + d_{Lj}^* \rangle] \quad (25)$$

In the circular basis, when leakages are known, crosshand phase calibration is synonymous with calibration of the absolute alignment of linear polarization<sup>7</sup> and requires an external source of known position angle. In the linear basis, an offset in the absolute alignment of the feeds (i.e. different observed  $\mathcal{U}_\psi$  and  $\mathcal{Q}_\psi$  in Equation 24) does not translate into a trivial change in crosshand phase. Thus, in the linear basis, crosshand phase and absolute position angle calibrations are not synonymous. However, unlike in the circular basis, if the linear antenna feeds are nominally aligned to the sky, an external source of known position angle is not formally required; variation in  $\mathcal{U}_\psi$  over parallactic angle for a linearly polarized source with unknown  $\mathcal{Q}$  and  $\mathcal{U}$  is sufficient to solve for  $\rho$ . As a result, calibration strategies in the linear basis typically need to obtain a first-pass solution for  $\mathbf{X}_r$ , assuming zero leakages, prior to solving for  $\mathbf{D}_r$ . Subsequent iteration is technically required (though typically negligible in practice) to account for leakages in the  $\mathbf{X}_r$  solve. In the circular basis,  $\mathbf{X}_r$  is not needed

<sup>7</sup> This is only strictly true for infinite signal to noise. In practice there will be a (likely) negligible yet non-zero bias between the recovered crosshand phase and the true overall position angle correction needed to correctly orient the crosshand phase frame.

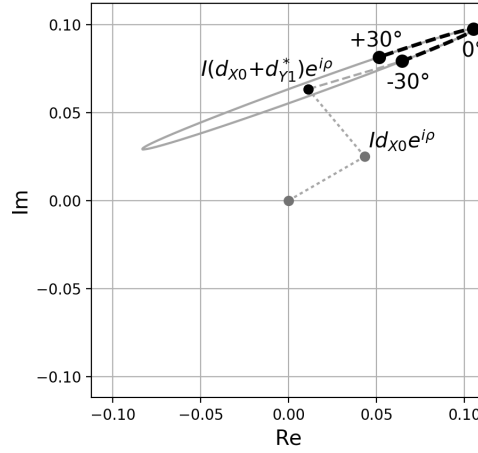


**Figure 1.** Path traced in complex plane by corrupted  $V_{XY}$  from Equation 17 on a single baseline ( $i = 0$ ,  $j = 1$ ) for a calibrator with  $(\mathcal{I}, \mathcal{Q}, \mathcal{U}, \mathcal{V}) = (1, 0, 0.1, 0)$ , instrumental leakages  $d_{X0}$  and  $d_{Y1}$  with moduli 0.05 and respective phases  $10^\circ$  and  $-110^\circ$ , and crosshand phase  $\rho = 20^\circ$ . The ellipse indicates the path traced by complete parallactic angle coverage, while the dashed curve indicates the path traced from  $\psi = -30^\circ$  to  $+30^\circ$  through  $0^\circ$ . The lighter-shaded dashed line connects the center of the ellipse to  $\psi = -30^\circ$ . The lighter-shaded dotted lines and points indicate how leakage from total intensity offsets the center of the ellipse from zero.

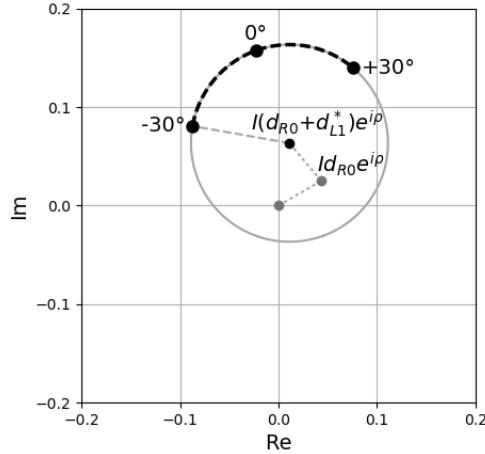


**Figure 2.** Path traced in complex plane by corrupted  $V_{RL}$  from Equation 21 for a single baseline. All calibrator and instrumental parameters are the same as described for Fig. 1, but with leakage subscripts  $X$  and  $Y$  replaced by  $R$  and  $L$ , respectively. Full parallactic angle coverage traces a circle, offset from zero by leakage from total intensity.

to solve for the leakages (crosshand phase simply imparts an overall rotational ambiguity) while  $\mathbf{D}_r$  is needed to optimally solve for  $\mathbf{X}_r$ . Thus circular basis calibration strategies typically solve for  $\mathbf{D}_r$  prior to  $\mathbf{X}_r$ .

Figures 1 and 2 illustrate how the respective corrupted cross hands from Equations 17 and 21 trace out geometric features in the complex plane as a function of parallactic angle coverage. In the linear

basis,  $\mathcal{U}_\psi$  moves along a rotated linear axis that is offset from the origin by leakages and broadened to become an ellipse due to the product of leakages with  $\mathcal{Q}_\psi$ . In the circular basis, a circle is drawn with center offset by the leakages (e.g. Conway & Kronberg 1969). These figures highlight degrees of freedom that must be calibrated. For example, calibration strategies in the circular basis that involve a polarized calibrator with unknown Stokes vector require at least 3 independent observations to solve for the d-terms (provided there are at least 3 baselines) as well as Stokes  $\mathcal{Q}$  and  $\mathcal{U}$ . Geometrically, this can be viewed as the need for 3 points to solve for the unknown origin and radius of a circle. When the Stokes vector is known a priori, only two observations are required to locate the origin (the known sense of rotation between the observations breaks the origin degeneracy). Degrees of freedom are examined more formally in the following section.

### 3.1. Degrees of freedom

Polarimetric calibration involves solving for the crosshand phase, leakage d-terms, and absolute alignment of linear polarization. External calibration is required to determine the absolute position angle in the same way that an interferometer cannot self-calibrate the absolute flux density level. Theoretically, to solve for all degrees of freedom in any basis that uses dual orthogonally polarized feeds, at least 3 distinct observations of calibrators with linearly independent Stokes vectors are required (Sault et al. 1996). This implies that at least 2 observations need to be on a polarized calibrator, at least 1 needs to be linearly polarized, and a circularly polarized calibrator is not essential. Observation of a linearly polarized calibrator over a range of parallactic angles can provide the necessary 3 distinct observations; rotation of the sky within the alt-az instrument frame enables the leakages and source polarization to be jointly solved. In practice, for circular polarization science in the linear feed basis, external (absolute) calibration of Stokes  $\mathcal{V}$  is also required<sup>8</sup> (e.g. Rayner et al. 2000) due to leakages being small (as a result of good engineering).

### 3.2. Absolute vs. relative leakages

Observational constraints may not always be available to solve for the d-terms unambiguously. For example, an unpolarized calibrator will yield solutions that are degenerate in the sum of leakage pairs, e.g.  $d_{Ri} + d_{Lj}^*$ . This corresponds to an undetermined Jones matrix which, in the small angle approximation, corresponds to a complex offset ( $\beta$ ) that can be added to one polarization and subtracted with conjugation from the other; e.g.  $d'_{pi} = d_{pi} + \beta$  and  $d'_{qj} = d_{qj} - \beta^*$  for all antennas (Sault et al. 1996). When solving for degenerate leakages, the real and imaginary components of the X or R feed leakages will be (arbitrarily) set to a constant (typically zero) on the gain reference antenna, effectively setting  $\beta$  to the negative of the true d-term on this antenna (e.g.  $\beta = -d_{p,ref}$ ). Leakage solutions degenerate in this manner are known as relative leakages. Absolute leakages are only accessible when additional observational constraints are available, e.g. from multiple observations of a polarized calibrator.

Relative leakages cannot substitute absolute leakages in the measurement equation without incurring errors. For calibration strategies that recover relative leakages, the degenerate nature of the

<sup>8</sup> To avoid the need for a circularly polarized calibrator in accord with the theoretical requirements presented above, second-order d-terms must be taken into account to break the imaginary-axis degeneracy otherwise present in the linearized  $\mathbf{DPV}^{mod}$  equations. However, even if these terms are included, non-singular solutions are likely to be produced in practice (small leakages, thermal noise, gain stability), in turn requiring absolute circular polarization calibration in the linear basis. To intuit why a similar issue does not arise in the circular basis, note that in the limit of large leakages there is no difference between observations in either basis, i.e. circular feeds can be thought of as linear feeds with high leakages (or leakages that act with crosshand phase to effectively operate as a quadrature hybrid coupler). In this case, the additional constraints available through the linear basis second-order terms become accessible.



solutions will manifest in the linear basis as an error in the position angle of linear polarization, an unknown degree of leakage between linearly and circularly polarized components, and gain errors in total intensity. In the circular basis there will be an unknown degree of leakage between linearly and circularly polarized components and gain errors will be produced in total intensity (Sault et al. 1996, or glean from equations presented in Section 3). As described earlier, this work will only focus on leakages accessible through the linearized cross hand visibilities. Accordingly, calibration strategies in the linear feed basis may recover relative or absolute leakages, depending on available observational constraints. Absolute leakages are accessible because the d-term sum degeneracy can be broken purely in the cross hands by  $\mathcal{Q}_\psi$ . Leakages in the circular basis, however, will always be relative; absolute leakages cannot be easily recovered without accessing the quadratic terms in the parallel hand visibilities or performing observations in which a subset of receivers are physically rotated (Sault & Perley 2013).

For completeness, it is worth noting that absolute leakages will often be quasi-absolute in practice because the measurement equation formalism assumes that the full signal path is characterized by a specific and limited set of effects. For example, the measurement equation under consideration may neglect terms regarding telescope analogue components (Price & Smirnov 2015) or direction dependent effects (Smirnov 2011). In practice, absolute leakages are non-singular solutions within the assumed framework.

#### 4. RESIDUAL ON-AXIS INSTRUMENTAL POLARIZATION

Strategies to calibrate instrumental leakage typically involve a single observation of an unpolarized calibrator, or multiple observations of a polarized calibrator spanning a range of parallactic angles. This section will present results from analytic derivations and Monte Carlo simulations with the aim to elucidate calibrator requirements so that subsequent observation of an unpolarized science target will deliver spurious on-axis polarization below a nominated threshold. For example, ALMA specifications require residual instrumental on-axis polarization to be below 0.1% of total intensity after calibration. Sections 4.1 and 4.2 will examine unpolarized and polarized calibrators, respectively, in both the linear and circular feed bases.

Throughout the following, an observation of a calibrator at a particular parallactic angle will be termed a *slice*. A slice may comprise one or more observational scans (in VLA parlance), but it will be assumed that parallactic angle is approximately constant throughout the slice and that the quoted signal to noise represents all combined scans within the slice. Note that, in practice, these concepts are linked: the ability to define the timespan over which parallactic angle can be considered constant is a function of signal to noise. Separation of these concepts is useful for framing the simulations. However, caution is required to ensure that the time needed to obtain a requisite signal to noise is not comparable to the parallactic angle range over which significant changes in residual leakage are predicted to occur.

A requirement for maximum spurious on-axis polarization translates to a calibration requirement for d-term accuracy. Taking  $\sigma_d$  as the characteristic d-term modulus error<sup>9</sup> and  $N_a$  as the number of antennas in the array, the approximate level of spurious on-axis linear ( $\mathcal{L}_\epsilon^{\text{LF}}$ ) or circular ( $\mathcal{V}_\epsilon^{\text{LF}}$ )

<sup>9</sup> If characteristic errors in either the real or imaginary d-term components are  $\sigma$ , then under Rayleigh statistics  $\sigma_d = \sqrt{\pi/2} \sigma$ .



polarization produced when observing an unpolarized source in the linear feed basis is

$$\mathcal{L}_\epsilon^{\text{LF}} \approx \mathcal{V}_\epsilon^{\text{LF}} \approx \mathcal{I} \frac{\sigma_d}{\sqrt{N_a}} . \quad (26)$$

Spurious elliptical polarization is

$$\mathcal{P}_\epsilon^{\text{LF}} \approx \mathcal{I} \sigma_d \sqrt{\frac{\pi}{2N_a}} . \quad (27)$$

In the circular feed basis, the level of spurious linear or elliptical polarization is

$$\mathcal{L}_\epsilon^{\text{CF}} \approx \mathcal{P}_\epsilon^{\text{CF}} \approx \mathcal{I} \sigma_d \sqrt{\frac{\pi}{2N_a}} . \quad (28)$$

No spurious circular polarization will be produced. Analytic derivations of these equations are presented in the Appendix. To illustrate, a requirement of 0.1% spurious on-axis linear polarization translates to  $\sigma_d \lesssim 0.6\%$  for ALMA ( $N_a = 40$ ) and  $\sigma_d \lesssim 0.4\%$  for the VLA ( $N_a = 27$ ). The equations above assume a worst-case scenario where the science target is observed within a single parallactic angle slice. For wider parallactic angle coverage the residual leakage will be smaller due to depolarization.

The equations above will now be used to translate  $\sigma_d$  into limits on anticipated spurious on-axis polarization for various calibration strategies.

#### 4.1. Unpolarized calibrators

A calibrator that is classified as unpolarized may in fact exhibit a low level of polarization, denoted by  $\mathcal{L}_{\text{true}}$ ,  $\mathcal{U}_{\psi,\text{true}}$ , or  $\mathcal{V}_{\text{true}}$  (other terms not needed below). Taking this into account, if leakage calibration is performed using an assumed unpolarized calibrator (resulting in relative leakages), the resulting d-term modulus error  $\sigma_d$  will be approximately

$$2(\sigma_d^{\text{LF}})^2 \approx \left( \frac{\mathcal{U}_{\psi,\text{true}}}{\mathcal{I}} \right)^2 + \left( \frac{\mathcal{V}_{\text{true}}}{\mathcal{I}} \right)^2 + \frac{N_a}{A^2} \quad (29)$$

in the linear feed basis and

$$2(\sigma_d^{\text{CF}})^2 \approx \left( \frac{\mathcal{L}_{\text{true}}}{\mathcal{I}} \right)^2 + \frac{N_a}{A^2} \quad (30)$$

in the circular feed basis, where  $A$  is the full-array dual-polarization total intensity signal to noise of the calibrator within the single spectral channel of interest. Derivations of these equations are presented in the Appendix. Note that the level of fractional polarization below which a source may be classified as ‘unpolarized’ depends on the telescope being used and the science goals of the observation. For science projects or telescopes that place a requirement on the acceptable level of spurious on-axis polarization following calibration, the equations above can be used to determine if a calibrator can be classed as unpolarized. Note that the dynamic range limitations arising from calibrator model errors presented by [Sault & Perley \(2014\)](#) may be relevant or even dominate considerations for some science goals.

Leakage calibration with an unpolarized calibrator can be performed using a single slice observation. In the circular basis, taking an example of an assumed unpolarized calibrator with true linear polarization  $\sim 1\%$  observed with the VLA at high signal to noise, the estimate from Equation 30 is

$\sigma_d \sim 0.7\%$ . The estimated spurious on-axis fractional polarization for an unpolarized science target observed over a small range in parallactic angle (e.g. snapshot) is then  $\sim 0.2\%$  from Equation 28. As another example, now in the linear basis using an unpolarized (or negligibly polarized) calibrator, the estimated spurious fractional linear polarization for an unpolarized science target is  $\sim 1/\sqrt{2A^2}$ .

## 4.2. Polarized calibrators

### 4.2.1. Linear basis

To calibrate leakages in the linear basis using a polarized source, observations are required over at least 3 parallactic angle slices if the Stokes vector is unknown a priori, or as little as a single slice if the Stokes vector is known. When the Stokes vector is unknown a priori, it needs to be solved for in addition to the d-terms and crosshand phase. For the case of a single slice observation on a calibrator with known Stokes vector, the available degrees of freedom only permit solving for relative leakages. In all other calibration strategies, absolute leakages can be recovered.

Simulations were performed to predict the level of spurious on-axis polarization and absolute position angle error resulting from a 1 (linearly polarized with Stokes known), 2 (linearly polarized with Stokes known), 3 (Stokes unknown), and 10 (Stokes unknown) slice strategy. Full details are presented in the Appendix, including a web link to the simulation code which has been made publicly available. This section will present the results for spurious polarization. Position angle errors will be reported in Section 5.1.

The simulations explore the accuracy with which the d-terms, crosshand phase, and calibrator polarization (when relevant) can be measured from the cross hand visibilities when a source is subjected to parallactic angle rotation in the presence of thermal noise. To solve for  $\sigma_d$ , the code focuses on a single cross product ( $V_{XY}$ ) and examines how well the d-term for the antenna and polarization under consideration can be recovered while taking into account all available  $N_a - 1$  baselines toward antenna  $i$ . The simulations assume an ALMA-like array with 40 antennas, typical d-term modulus of 1.5%, and mechanical feed alignment uncertainty of  $2^\circ$  per antenna (Cortes et al. 2015); the alignment uncertainty is only used for position angle analysis (see Section 5.1).

For multi-slice strategies, the first slice is assumed to be observed at maximum  $|\mathcal{U}_\psi|$ . This produces approximately worst-case results, compared to for example symmetric coverage about maximum  $|\mathcal{U}_\psi|$ , because the arc traced along the ellipse in the complex plane for a cross hand visibility is minimized, leading to poorer constraints on recovered parameters. Note that truly worst-case results would arise from limited coverage about  $\mathcal{U}_\psi = 0$ , in which case crosshand phase would be degenerate and calibration would fail. The simulations use Monte Carlo sampling to recover the distribution of  $\sigma_d$ , from which the 95<sup>th</sup> percentile is measured and converted to spurious linear polarization using Equation 26. Two scenarios have been examined, the first for a calibrator exhibiting 3% fractional linear polarization and the second with fraction 10%.

Results for the 1 slice strategy are presented in Figure 3. The displayed spurious fractional polarization trend is practically indistinguishable from the analytic prediction for an unpolarized calibrator described at the end of Section 4.1. The reason is because d-term errors arising from crosshand phase errors, drawn from data where all baselines are combined in the solve, always remain practically negligible compared to thermal noise in the subset of baselines from which individual d-terms are effectively solved. Thus the fractional polarization of the calibrator will not practically affect the

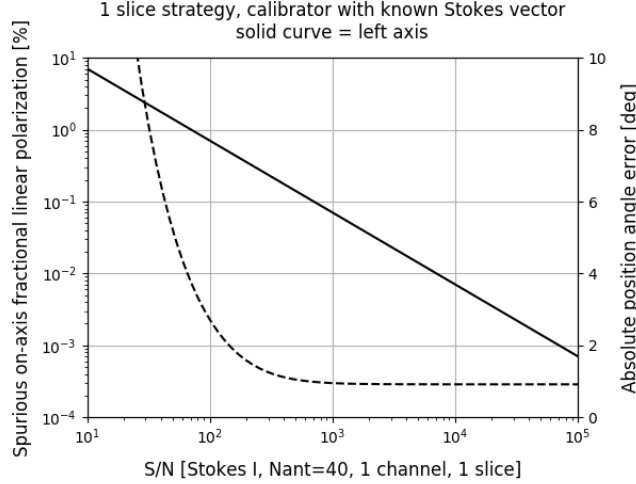


**Figure 3.** Results from simulations showing 95<sup>th</sup> percentile spurious on-axis fractional linear polarization and absolute position angle error, predicted to arise within 1 spectral channel when a linear basis telescope is calibrated using a single slice observation of a polarized calibrator with known Stokes vector. The indicated position angle error must be added in quadrature with a target source’s statistical error to obtain its total position angle error. The displayed curves are from simulations with a 3% linearly polarized calibrator. Results from the 10% case are not displayed as they are indistinguishable.

result (unless it approaches 100%); curves obtained for the 3% and 10% fractionally polarized cases are indistinguishable.

Results for the 2, 3, and 10 slice strategies are displayed in Figure 4. The distorted contours seen at very small or very large parallactic angle coverages in panels where the Stokes vector is unknown are artifacts that can be ignored; these are the result of simplifications in the code that are localized to these regions of parameter space (the temporal ordering of points is ignored). The plots indicate that, in general for a given calibrator, total parallactic angle coverage of approximately 30° is sufficient to maximize calibration accuracy. Beyond 30°, additional parallactic angle coverage only delivers minor improvements. In the 2 slice strategy, separation of slices beyond approximately 70° will lead to degraded calibration solutions and increased spurious polarization. The spurious polarization levels are found to be smaller when using a more highly fractionally polarized calibrator, as expected.

#### 4.2.2. Circular basis

To calibrate leakages in the circular basis using a polarized source, observations are required over at least 2 or 3 parallactic angle slices depending on whether the Stokes vector is known a priori or not, respectively. When unknown a priori, the Stokes vector needs to be solved for in addition to the d-terms.

Monte Carlo simulations similar to those described for the linear basis were performed to predict the level of spurious on-axis polarization and absolute position angle error resulting from a 2 (linearly polarized with Stokes known), 3 (Stokes unknown), and 10 (Stokes unknown) slice strategy. To solve for  $\sigma_d$ , the code focuses on a single cross product ( $V_{RL}$ ) and examines how well the d-term for the antenna and polarization under consideration can be recovered while taking into account all available  $N_a - 1$  baselines toward antenna  $i$ . The simulations assume a VLA-like array with 27 antennas. Full details are presented in the Appendix, including a web link to the publicly available simulation code.

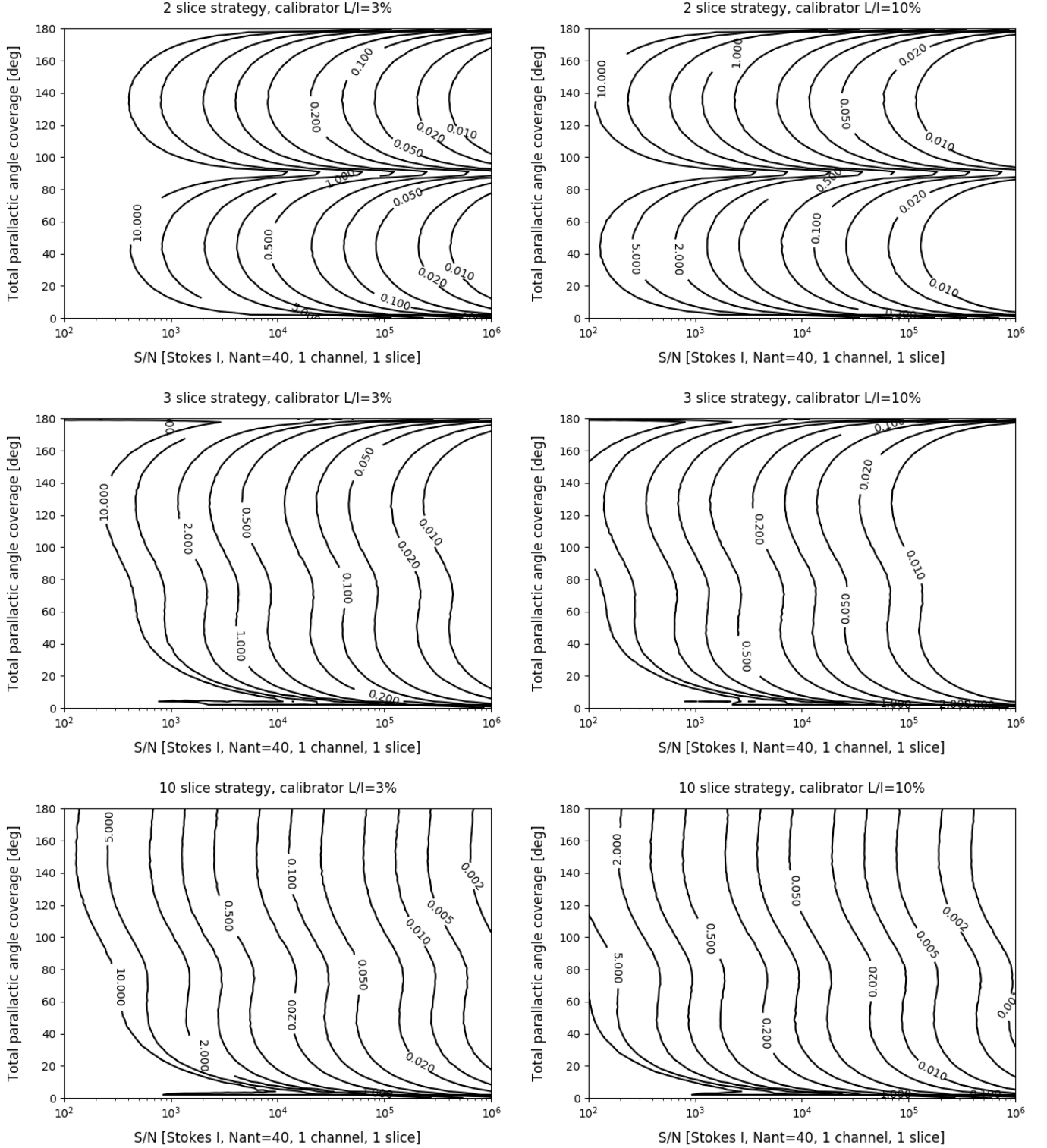


**Figure 4.** Results from simulations showing 95<sup>th</sup> percentile spurious on-axis fractional linear polarization (percent) for an unpolarized target arising from different calibration strategies with a linear basis telescope. The simulations assume an ALMA-like array with 40 antennas. Top row: 2 slice strategy with polarization known a priori. Middle row: 3 slice strategy with unknown polarization. Bottom row: 10 slice strategy with unknown polarization. Panels in the left and right columns show results obtained using a calibrator with 3% or 10% fractional linear polarization, respectively. Abscissa: Full-array dual-polarization total intensity signal to noise within 1 spectral channel and 1 slice. Ordinate: Total parallactic angle coverage; divide by 1 less than the number of slices to get the inter-slice separation. The distorted contours seen at very small and large parallactic angle coverages in some panels are the result of coding artifacts and should be ignored.

This section will present the results for spurious polarization, which is calculated in the code by taking the recovered 95<sup>th</sup> percentile  $\sigma_d$  and performing a conversion using Equation 28. Position angle errors will be reported in Section 5.2.

Results are displayed in Figure 5. The distorted contours seen at small parallactic angle coverages in panels where the Stokes vector is unknown are artifacts that can be ignored; they are the result of simplifications in the code that are localized to these regions of parameter space (the temporal ordering of points is ignored). The plots demonstrate that, as expected, a floor is reached at low signal to noise where no amount of parallactic angle coverage can make up for the dominant randomizing influence of thermal noise. This is not seen in the linear basis results because the method of solving for the d-terms is different (see Appendix; linear basis calibration can take advantage of prior crosshand phase calibration). Note that the displayed signal to noise range differs between the linear and circular basis plots.

The 2 slice strategy reveals the counter-intuitive result that a calibrator with larger fractional polarization will, at low signal to noise, result in higher spurious polarization than a calibrator with low fractional polarization. This is because the fractional polarization is a fixed known quantity when signal to noise is defined for total intensity; solving for the origin of a circle with fixed radius in the presence of thermal noise leads to larger fractional errors when the radius is larger. Indeed, this trend continues to the case of unpolarized calibrators; spurious polarization limits are even smaller when observing an unpolarized calibrator at the equivalent signal to noise. For the 3 and 10 slice strategies, the Stokes vector is not known a-priori, so calibrators with higher fractional polarization deliver better quality solutions than lower ones, as expected.

The results presented here indicate that, in general, when the Stokes vector of the leakage calibrator is known a priori, total parallactic angle coverage of approximately 30° is sufficient to maximize calibration accuracy. Additional coverage is not found to deliver significant improvements. In the 2 slice strategy, separation of slices beyond approximately 70° will lead to degraded calibration solutions and increased spurious polarization. These match findings for the linear basis presented in Section 4.2.1. However, when the Stokes vector is unknown in the circular basis, the minimum coverage requirement increases to approximately 90°.

## 5. POSITION ANGLE ERRORS

As with leakage calibration, observational constraints may not always be available to perform absolute position angle calibration. If absolute position angles are not calibrated, scientifically useful data may still result, for example if the spectrum of fractional polarization is of interest, or in particular for the linear basis if position angles are only partially calibrated. The following sections explore position angle errors in the linear and circular bases.

### 5.1. Linear basis

In the linear basis, calibration strategies must recover  $\text{Re}(d_{Xref})$ , the real part of the d-term on the X feed of the gain reference antenna, in order to provide self-consistent alignment to the assumed sky frame. If relative leakages are recovered, a systematic contribution to position angle errors will be imposed, given by the magnitude of  $\text{Re}(d_{Xref})$ . For example,  $\text{Re}(d_{Xref}) \sim 2\%$  implies a systematic position angle error contribution of  $\sim 1^\circ$ . This relationship can be derived by considering how the unaccounted degree of freedom associated with the true value of  $d_{Xref}$  will be absorbed by  $\mathcal{Q}_\psi$  and  $\mathcal{U}_\psi$  in Equations 16–19 when relative leakages ( $r$ ) are utilized, compared with their original values

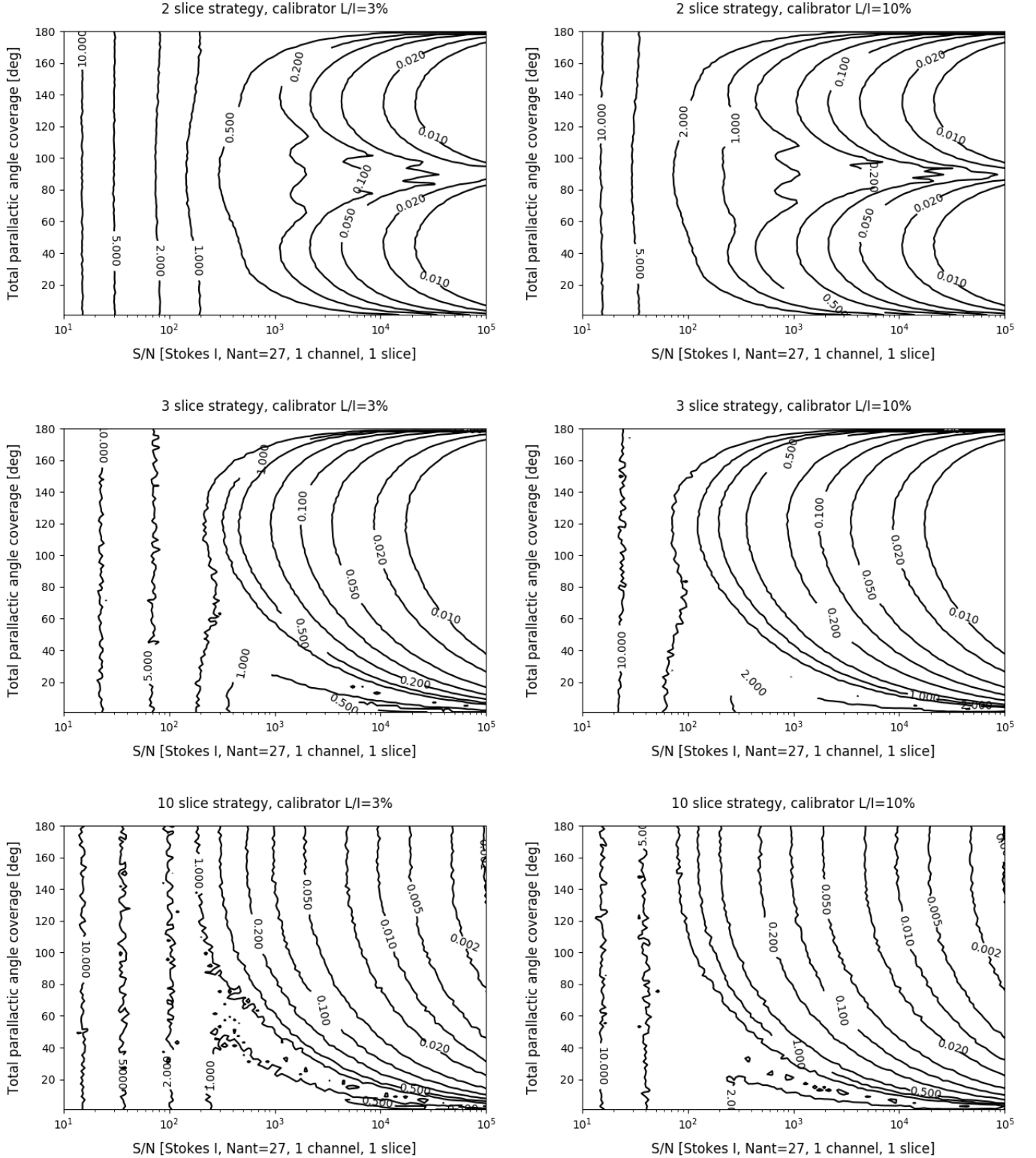


**Figure 5.** Results from simulations showing 95<sup>th</sup> percentile spurious on-axis fractional linear polarization (percent) for an unpolarized target arising from different calibration strategies with a circular basis telescope. The simulations assume a VLA-like array with 27 antennas. Panel layout and axes are the same as Figure 4. The distorted contours seen at small parallactic angle coverages in some panels, in which a valley is produced, are the result of coding artifacts and should be ignored.



calculated in the presence of absolute leakages ( $a$ ). The differences are  $\mathcal{Q}_{\psi_r} - \mathcal{Q}_{\psi_a} = -2 \operatorname{Re}(d_{X \text{ ref}}) \mathcal{U}_{\psi_a}$  and  $\mathcal{U}_{\psi_r} - \mathcal{U}_{\psi_a} = 2 \operatorname{Re}(d_{X \text{ ref}}) \mathcal{Q}_{\psi_a}$ . The position angle difference is then  $\operatorname{Re}(d_{X \text{ ref}})$  in the small angle approximation.

The above calculation can also be used to estimate position angle errors resulting from d-term statistical measurement errors. The resulting worst-case position angle error is approximately  $\sigma_d$ , i.e. if all d-terms were made relative to an offset of this magnitude.

An additional systematic position angle error will arise due to each antenna in the array exhibiting a non-zero mechanical feed alignment uncertainty about the nominal alignment (where the nominal alignment is a specified angle between the  $X$  feed and the meridian at  $\psi = 0$ ). Thus, in general, the standard error in the mean of feed alignments over the array will be non-zero, leading to an offset between the assumed and true sky frames. In turn, measured Stokes  $\mathcal{Q}$  and  $\mathcal{U}$  will be slightly rotated versions of their true values. Leakage calibration will remain internally consistent for both relative and absolute cases, accounting for the misaligned feeds. However, the systematic misalignment over the array will remain uncorrected. External position angle calibration, using a source with known Stokes vector to adjust  $\operatorname{Re}(d_{X \text{ ref}})$  and perform relative application to all other leakages, is required to account for this offset and provide true absolute position angle calibration. For statistically independent feed misalignments over the array (not necessarily true in practice due to correlated installation procedures), the systematic position angle uncertainty contribution will be approximately  $\phi/\sqrt{N_a}$ , where  $\phi$  is the characteristic alignment uncertainty per antenna. To illustrate, this is  $\lesssim 2^\circ/\sqrt{40} \approx 0.3^\circ$  for ALMA.

Thus, total systematic position angle uncertainty (i.e. frame error) for a target source in the linear basis is the quadrature sum of up to 3 terms: systematic error when relative leakages are recovered (i.e. when  $d_{X \text{ ref}}$  is artificially set to complex zero) given by the magnitude of the true  $\operatorname{Re}(d_{X \text{ ref}})$ , systematic error from d-term measurement errors, and systematic feed misalignment error. The relationship is

$$\theta_{\text{syst.}}^2 \approx [\operatorname{Re}(d_{X \text{ ref}})]^2 + \sigma_d^2 + \frac{\phi^2}{N_a} . \quad (31)$$

Total position angle error can then be calculated for a target source by combining the total systematic error above with statistical error (i.e. in-frame error) associated with the signal to noise of detection.

In this section, and in the simulation code developed for this work, it will be assumed that linear basis calibration does *not* include absolute position angle calibration (i.e. the final term in Equation 31 will be included in all calculations). This is regardless of whether relative or absolute leakages are recovered, or importantly whether a linearly polarized calibrator with known Stokes vector is available or not. This is consistent with typical data reduction procedures for major telescopes such as ALMA and the Australia Telescope Compact Array (ATCA). Results for position angle errors can therefore be compared directly between the calibration strategies examined in this work. To include the effect of absolute position angle calibration in any of the results, subtract  $\phi/\sqrt{N_a}$  in quadrature, where  $\phi = 2^\circ$  is the value assumed in the simulations. Systematic position angle errors resulting from the use of unpolarized and polarized calibrators will now be examined.

If an unpolarized calibrator is utilized for polarization calibration, relative leakages will be recovered. The total systematic position angle error is then estimated using Equation 31, including the first term. A worst-case estimate for the second term is given by  $\sigma_d^2 = N_a/(2A^2)$  from Equation 29.



Position angle errors arising from calibration strategies involving a polarized calibrator were examined using the 1, 2, 3, and 10 slice Monte Carlo simulations introduced in Section 4.2.1. Position angle errors were calculated in a similar manner to leakages, taking the recovered 95<sup>th</sup> percentile  $\sigma_d$  from the simulations and evaluating the total systematic position angle error using Equation 31. The first term in Equation 31 was only included for the 1 slice simulation; the other calibration strategies recover absolute leakages.

The result from the 1 slice simulation is displayed in Figure 3. The asymptotic behavior is due to the final term in Equation 31. As with the spurious leakage curve, the overall position angle error curve is practically indistinguishable from the analytic prediction for an unpolarized calibrator that may be obtained by combining Equation 29 with Equation 31.

Results from the 2, 3, and 10 slice strategies are displayed in Figure 6. Similar conclusions regarding parallactic angle coverage may be drawn as for leakages described in Section 4.2.1.

### 5.2. Circular basis

Position angle calibration in the circular basis is tied to crosshand phase calibration. This requires a polarized calibrator.

To examine position angle errors resulting from crosshand phase calibration, a Monte Carlo simulation was performed based on Equation 25. The result is presented in Figure 7. To illustrate interpretation of this figure, consider position angle calibration with the VLA within a 2 MHz channel at 3 GHz using 3C48 ( $\sim 10$  Jy,  $\sim 2\%$  fractional linear polarization). A signal to noise ratio in excess of 300 is required to limit systematic position angle uncertainty to within  $0.1^\circ$ . This translates to an on-source time approaching 4 min. For  $0.3^\circ$  uncertainty, the required on-source time is  $\sim 30$  sec.

## 6. CONCLUSIONS

The mathematical framework for describing interferometric radio polarimetry does not readily permit quantitative calculation of post-calibration residuals for specific observational calibration strategies. This work has bridged this gap through the presentation of analytic derivations and results from Monte Carlo simulations. In general, worst-case errors have been assumed. Thus, in practice, residual leakage and position angle errors are likely to be smaller.

This work has focused on arrays that comprise alt-az antennas with common feeds over which parallactic angle is approximately uniform, such as ALMA and the VLA. The simulation code has been made publicly available to support potential extension, for example to investigate mixed basis arrays (e.g. Martí-Vidal et al. 2016), VLBI, calibration strategies using resolved polarization calibrators, or a more detailed examination of circular polarimetry.

This work was motivated by the need to implement automated polarization data reduction capabilities within the CASA integrated pipelines for ALMA<sup>10</sup> and the VLA<sup>11</sup>. As a result, this work forms part of ALMA Memo 603, equivalently referenced as EVLA Memo 201 (Hales 2017). This memo contains extensive additional material, including a general classification system for polarization calibrators, and detailed step by step procedures for performing a suite of polarimetric calibration strategies in the linear and circular bases.

<sup>10</sup> <https://almascience.nrao.edu/documents-and-tools/>

<sup>11</sup> <https://science.nrao.edu/facilities/vla/data-processing/pipeline>

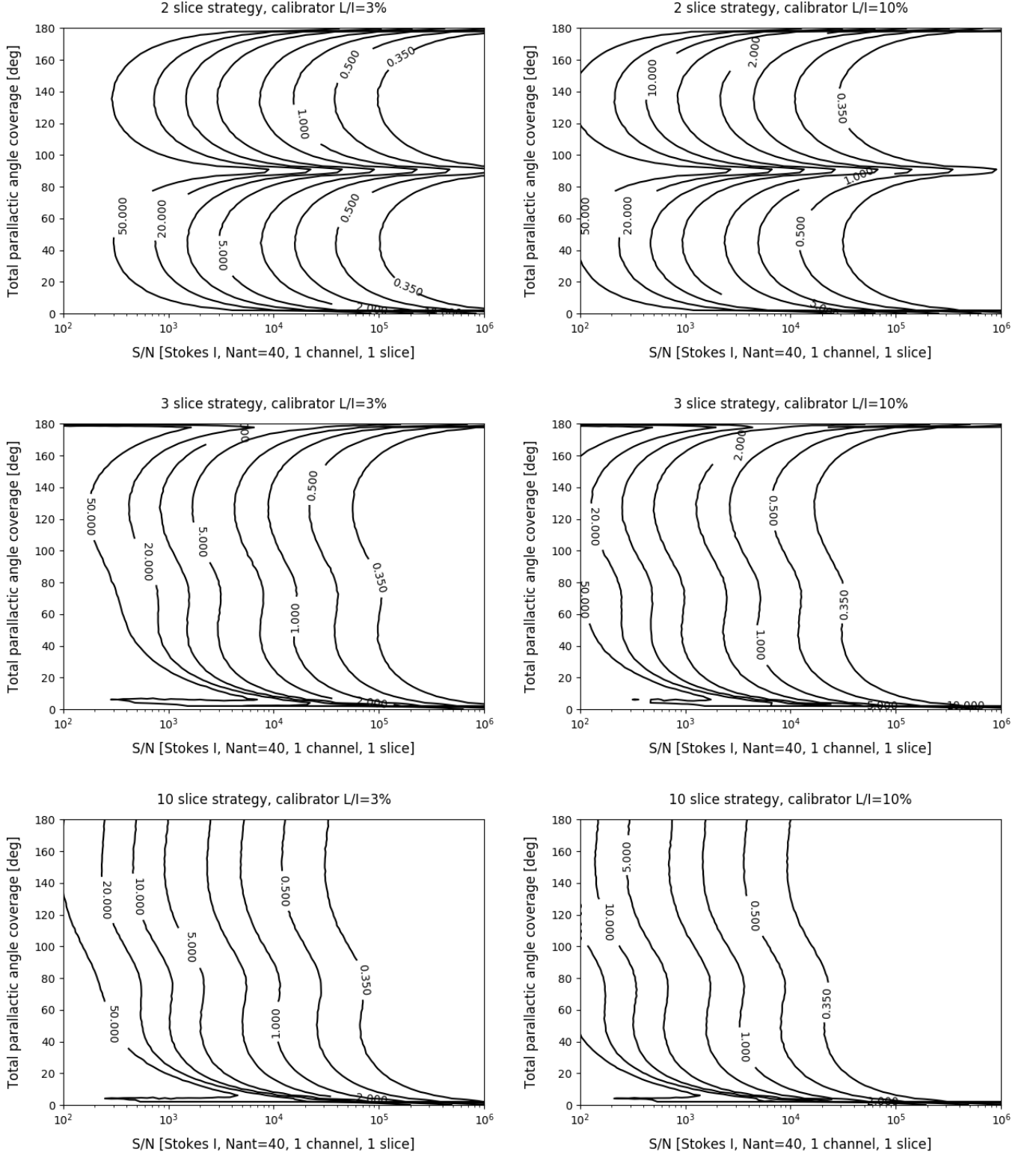


**Figure 6.** Results from simulations showing 95<sup>th</sup> percentile systematic position angle error (degrees) arising from different calibration strategies with a linear basis telescope. Panel layout and axes are the same as Figure 4. The distorted contours seen at very small and large parallactic angle coverages in some panels are the result of coding artifacts and should be ignored.

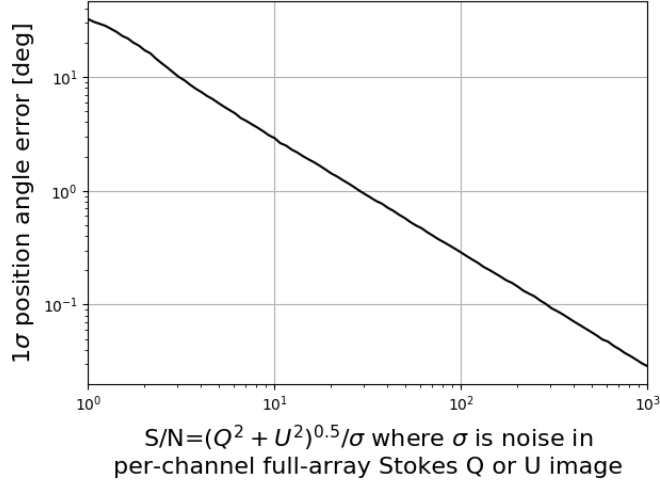


**Figure 7.** Result from simulation showing systematic position angle error for calibration with a circular basis telescope. Abscissa: Full-array dual-polarization linear polarization signal to noise within 1 spectral channel. Ordinate: Standard error in systematic position angle error.

I thank the following for insightful discussions: George Moellenbrock, Bob Sault, Brian Kent, Lindsey Davis, Vincent Geers, Kumar Golap, Jeff Kern, Joe Masters, and Claire Chandler. I thank the ALMA Integrated Science Team for reviewing this document under the context of CASA automated pipeline design. I thank the anonymous referee for their thoughtful review which led to the improvement of this paper. The National Radio Astronomy Observatory is a facility of the National Science Foundation operated under cooperative agreement by Associated Universities, Inc. This project has received funding from the European Union’s Horizon 2020 research and innovation programme under the Marie Skłodowska-Curie grant agreement No 705332.

*Software:* Simulation code (Hales 2017), CASA (McMullin et al. 2007)

## APPENDIX

### A. RESIDUAL ON-AXIS INSTRUMENTAL LEAKAGE

Section 4 presented equations to predict the level of spurious on-axis polarization that will be observed for an intrinsically unpolarized target source following the application of imperfect d-term calibration solutions. Using these relationships, Section 4.1 presented equations to predict the d-term measurement errors, and in turn the level of spurious polarization, that will result following leakage calibration when using a polarized calibrator that is assumed to be unpolarized. Similarly, Section 4.2 presented results from simulations in which d-term measurement errors, and ultimately spurious polarization signatures, were predicted empirically for calibration schemes involving observation of a polarized calibrator over a range of parallactic angles (slices). Derivations for all equations, and details of the simulations, are presented below for the circular and linear feed bases.

#### A.1. Circular basis

Stokes  $Q$  is formed by

$$Q = 0.5 \operatorname{Re} \left[ \langle e^{+i2\psi} V_{RL} \rangle + \langle e^{-i2\psi} V_{LR} \rangle \right]. \quad (\text{A1})$$

If d-terms are recovered with measurement errors  $\Delta d$  (statistical or systematic in origin), an unpolarized target will be observed with spurious fractional polarization

$$\frac{\mathcal{Q}_\epsilon}{\mathcal{I}} = 0.5 \operatorname{Re} \left[ \langle e^{+i2\psi} (\Delta d_{Ri} + \Delta d_{Lj}^*) \rangle + \langle e^{-i2\psi} (\Delta d_{Li} + \Delta d_{Rj}^*) \rangle \right]. \quad (\text{A2})$$

The worst-case spurious polarization will therefore occur for a target observed with limited parallactic angle coverage. If the science target is integrated over a wide range in parallactic angle, then the level of spurious polarization predicted in the following should be treated as an upper limit. Taking the worst-case scenario of approximately constant parallactic angle, and noting that there are only  $N_a$  independent d-terms per polarization over the array, the relationship above can be rewritten in a statistical sense as

$$\frac{\mathcal{Q}_\epsilon}{\mathcal{I}} \approx \operatorname{Re} \left[ \frac{1}{N_a} \sum \Delta d_{Ri} + \Delta d_{Li} \right]. \quad (\text{A3})$$

For characteristic d-term modulus error  $\sigma_d$ , the variance in  $\operatorname{Re}[\Delta d]$  is given by  $\sigma_d^2/2$ . The variance in Equation A3 is then estimated as

$$\operatorname{var} \left( \frac{\mathcal{Q}_\epsilon}{\mathcal{I}} \right) \approx \frac{\sigma_d^2}{N_a}. \quad (\text{A4})$$

Similar analysis for fractional  $\mathcal{U}_\epsilon$  yields the same result. The predicted level of spurious on-axis fractional linear polarization is then Rayleigh distributed with mean

$$\frac{\mathcal{L}_\epsilon}{\mathcal{I}} \approx \sqrt{\frac{\pi}{2N_a}} \sigma_d. \quad (\text{A5})$$

No spurious circular polarization is predicted ( $\mathcal{V}_\epsilon = 0$ ) because its evaluation does not include any leakage products with total intensity (to first order). The results above are presented in Section 4.

If a polarized calibrator is assumed to be unpolarized for leakage calibration, any true (linear) polarization will lead to corruption of the measured leakages. The difference between observed and true cross hand visibilities for a single baseline is given by

$$\Delta V_{RL} = \mathcal{I} (\Delta d_{Ri} + \Delta d_{Lj}^*) - (\mathcal{Q}_{\text{true}} + i\mathcal{U}_{\text{true}})e^{-i2\psi}. \quad (\text{A6})$$

Note that non-zero  $\mathcal{V}_{\text{true}}$  will not affect relative leakages that are calculated using only cross hand data (to first order). The equation above is effectively constrained by  $N_a - 1$  baselines toward antenna  $i$ , in which case

$$\Delta d_{Ri} + \frac{1}{N_a - 1} \sum_{j=1}^{N_a-1} \Delta d_{Lj}^* = \frac{\mathcal{Q}_{\text{true}} + i\mathcal{U}_{\text{true}}}{\mathcal{I}} e^{-i2\psi} + \frac{1}{N_a - 1} \sum_{j=1}^{N_a-1} \frac{\Delta V_{RL}}{\mathcal{I}}. \quad (\text{A7})$$

In this construction, the leakages will soak up the source polarization, leaving the  $\Delta V_{RL}$  term consisting of only thermal noise. As a result, its average in the right side of the equation can be represented by a vector with characteristic magnitude  $\sqrt{N_a}/A$ , where  $A$  is the full-array dual-polarization total intensity signal to noise of the calibrator within the single spectral channel of interest. The first term in the left side of the equation has characteristic magnitude  $\sigma_d$ . The importance of the next term, containing the average over d-terms, depends on whether the d-terms are correlated between

antennas or not. When random errors dominate over systematics from the true source polarization (e.g. for small  $A$ ), the recovered d-term errors will be effectively uncorrelated. In this case, the term can be viewed as a vector-averaged sample of ( $\sigma_d$ -scale) error vectors, in which case its contribution will be negligible<sup>12</sup> and can be ignored. When source polarization systematics dominate (e.g. for large  $A$ ), the d-terms will be correlated and the average cannot be ignored. This can be crudely accommodated by replacing  $\Delta d_{Lj}^*$  with  $\Delta d_{Ri}$ , in which case the left side of Equation A7 can be approximated by  $2\Delta d_{Ri}$ . Thus, the estimated  $\sigma_d$  will be half of the value recovered when assuming uncorrelated d-terms. Given the simplistic nature of this calculation, the larger estimate for  $\sigma_d$  will be adopted; its estimated value presented below should therefore be treated as an upper limit.

By noting that contributions to  $\sigma_d$  on the right side of Equation A7 represent projections onto a 1D vector given by the true d-term (requiring adjustment to variances by factor 1/2), and by treating the true polarization as a DC offset with magnitude  $\mathcal{L}_{\text{true}}$ , the d-term modulus error can be estimated in rms-fashion as

$$\sigma_d \approx \sqrt{\frac{1}{2} \left( \left[ \frac{\mathcal{L}_{\text{true}}}{\mathcal{I}} \right]^2 + \frac{N_a}{A^2} \right)}. \quad (\text{A8})$$

The resulting estimate for spurious fractional linear polarization is then obtained using Equation A5, giving

$$\frac{\mathcal{L}_\epsilon}{\mathcal{I}} \approx \sqrt{\frac{\pi}{4N_a} \left( \left[ \frac{\mathcal{L}_{\text{true}}}{\mathcal{I}} \right]^2 + \frac{N_a}{A^2} \right)}. \quad (\text{A9})$$

These results are reported in Section 4.1. Note that if the leakage calibrator is observed over a wide range in parallactic angle (atypical for an assumed unpolarized calibrator), then the predicted spurious polarization should be treated as an upper limit (in addition to the motivation described earlier).

Figure 5 presents estimates of spurious polarization for calibration strategies involving parallactic angle coverage of a polarized leakage calibrator. To obtain these results, a Monte Carlo simulation code was developed to estimate  $\sigma_d$  and perform conversion using Equation A5. The code focuses on the theoretical aspects discussed in this document by approximating the behaviour of the generalized solvers that exist within software such as CASA, as described below. Full CASA-based (or other package) simulations using mock or real data were not considered for this work due to the potential for introducing a host of unwanted systematics, which could readily bias interpretation of the fundamental attributes under investigation. The simulation code is publicly available at <https://github.com/chrishales/polcalsims> (Hales 2017).

To estimate  $\sigma_d$  for the calibration schemes examined, the code performs Monte Carlo sampling and examines the distribution of errors recovered when attempting to solve for the d-term for a single polarization on a single antenna. To do this, the code focuses on a single cross product (e.g.  $V_{RL}$ ) and examines how well the d-term under consideration can be recovered while taking into account all available  $N_a - 1$  baselines toward antenna  $i$ . The relevant relationship is given by Equation A7, with the sum over  $\Delta d_{Lj}^*$  assumed to be negligible. The true source polarization is injected with the

<sup>12</sup> To demonstrate, consider the variance for a sample of unit vectors with random orientations projected along a 1D axis. This is given by  $0.5/(N_a - 1)$ . The standard error for the left side of the equation can therefore be approximated by  $\sigma_d \sqrt{1 + 0.5/(N_a - 1)}$ . This indicates a negligible difference of  $< 12\%$  for  $N_a > 2$ .

appropriate thermal noise at slices that are, for simplicity, spaced equally over the total parallactic angle span under consideration.

Calibration strategies involving a polarized calibrator with unknown Stokes vector require at least 3 statistically independent slices to solve for the d-term (error) as well as Stokes  $\mathcal{Q}$  and  $\mathcal{U}$ . Geometrically, this can be viewed as the need for 3 points to solve for the unknown origin and radius of a circle (see Fig. 2). When the Stokes vector is known a priori, only two slices are required to locate the origin (the origin degeneracy is broken by the known sense of rotation between the slices). For simplicity, the simulation code does not take into account the sense of rotation between points. As a result, the portion of parameter space containing observations at modest signal to noise ratios over small total parallactic angle ranges displays much noisier solutions than those likely to be recovered in production code. This effect is not significant; results throughout the remaining parameter space are not affected.

The code recovers the distribution of d-term errors for each sampled point in the signal to noise and parallactic angle coverage parameter space. Rather than reporting the mean of this distribution to represent  $\sigma_d$ , the code reports the 95<sup>th</sup> percentile in order to better accommodate the slightly non-Gaussian nature of the results in a conservative manner. This is consistent with the comments earlier to interpret results as upper limits.

#### A.2. Linear basis

Assuming perfect crosshand phase measurement,  $\mathcal{U}_\psi$  is formed by

$$\mathcal{U}_\psi = 0.5 \operatorname{Re} [\langle V_{XY} \rangle + \langle V_{YX} \rangle] . \quad (\text{A10})$$

The presence of d-term measurement errors will cause an unpolarized target to exhibit spurious fractional linear polarization, described statistically as

$$\frac{\mathcal{U}_{\psi,\epsilon}}{\mathcal{I}} \approx \operatorname{Re} \left[ \frac{1}{N_a} \sum^{N_a} \Delta d_{Xi} + \Delta d_{Yi} \right] . \quad (\text{A11})$$

The worst-case spurious polarization will occur for a target observed with limited parallactic angle coverage. Assuming the worst-case scenario of approximately constant parallactic angle, the variance in Equation A11 is then estimated as

$$\operatorname{var} \left( \frac{\mathcal{U}_{\psi,\epsilon}}{\mathcal{I}} \right) \approx \frac{\sigma_d^2}{N_a} . \quad (\text{A12})$$

Similar analysis for fractional  $\mathcal{V}_\epsilon$  yields the same result. No spurious  $\mathcal{Q}_\psi$  will be produced because its evaluation does not include any leakage products with total intensity. As a result, the predicted level of spurious on-axis fractional linear or circular polarization is given by

$$\frac{\mathcal{L}_\epsilon}{\mathcal{I}} \approx \frac{\mathcal{V}_\epsilon}{\mathcal{I}} \approx \frac{\sigma_d}{\sqrt{N_a}} . \quad (\text{A13})$$

The predicted level of spurious fractional elliptical polarization is then Rayleigh distributed with mean

$$\frac{\mathcal{P}_\epsilon}{\mathcal{I}} \approx \sqrt{\frac{\pi}{2N_a}} \sigma_d . \quad (\text{A14})$$

These results are presented in Section 4.

The results presented in Section 4.1 regarding calibration with a polarized yet assumed-unpolarized calibrator can be derived in the same way as presented earlier for the circular feed basis, but replacing  $\mathcal{L}_{\text{true}}^2$  with  $\mathcal{U}_{\psi,\text{true}}^2 + \mathcal{V}_{\text{true}}^2$  in Equation A8. For the linear basis derivation here, it will be assumed that the product of  $\mathcal{Q}_{\psi,\text{true}}$  with leakages in the cross hand visibilities is always negligible. This will not always be true in practice, but in such cases the contribution from thermal noise ( $A$ ) is likely to dominate. The resulting estimates of spurious fractional linear or circular polarization are then obtained using Equation A13, giving

$$\frac{\mathcal{L}_\epsilon}{\mathcal{I}} \approx \frac{\mathcal{V}_\epsilon}{\mathcal{I}} \approx \sqrt{\frac{1}{2} \left( \left[ \frac{\mathcal{U}_{\psi,\text{true}}}{\mathcal{I}} \right]^2 + \left[ \frac{\mathcal{V}_{\text{true}}}{\mathcal{I}} \right]^2 + \frac{N_a}{A^2} \right)}. \quad (\text{A15})$$

The estimate of spurious fractional elliptical polarization is obtained using Equation A14, giving

$$\frac{\mathcal{P}_\epsilon}{\mathcal{I}} \approx \sqrt{\frac{\pi}{4N_a} \left( \left[ \frac{\mathcal{U}_{\psi,\text{true}}}{\mathcal{I}} \right]^2 + \left[ \frac{\mathcal{V}_{\text{true}}}{\mathcal{I}} \right]^2 + \frac{N_a}{A^2} \right)}. \quad (\text{A16})$$

Figure 4 presents estimates of spurious polarization for calibration strategies involving parallactic angle coverage of a polarized leakage calibrator. To obtain these results, simulation code was developed with similar characteristics to those described earlier for the circular feed basis. Differences are described below. The simulation code is publicly available at <https://github.com/chrishales/polcalsims> (Hales 2017).

The code focuses on a single cross product (e.g.  $V_{XY}$ ) and examines how well the d-term for the antenna and polarization under consideration can be recovered while taking into account all available  $N_a - 1$  baselines toward antenna  $i$ . Unlike in the circular basis, measurement of the crosshand phase is required here prior to solving for leakages. The linear basis simulation code therefore takes into account crosshand phase measurement errors due to thermal noise when calculating the d-term measurement errors. The code does not account for errors in crosshand phase measurement due to the as-yet unknown leakages, which are assumed to be zero for this calculation (such errors are typically negligible in the baseline-averaged crosshand phase solve, minimizing the need for iteration). The code assumes that Stokes  $\mathcal{V}$  is zero for all calibrators. The relevant equation is then a modified version of Equation 17,

$$\frac{1}{N_a - 1} \sum \frac{V_{XY}}{\mathcal{I}} = \frac{\mathcal{U}_\psi}{\mathcal{I}} e^{i\rho} + \left(1 - \frac{\mathcal{Q}_\psi}{\mathcal{I}}\right) e^{i\rho} d_{Xi} + \left(1 - \frac{\mathcal{Q}_\psi}{\mathcal{I}}\right) \frac{e^{i\rho}}{N_a - 1} \sum d_{Yj}^* + \frac{1}{N_a - 1} \sum \frac{\sigma_{V_{XY}}}{\mathcal{I}} \quad (\text{A17})$$

in which thermal noise in  $V_{XY}$  is explicitly included, denoted by  $\sigma_{V_{XY}}$ . For all multi-slice observing strategies, the simulation code assigns each of the d-terms that appear in the equation above with a user-defined characteristic amplitude and random phase. The error in recovering the input  $d_{Xi}$  is then ultimately recorded.

For simplicity, the code assumes that the first observed slice for each calibration strategy is at zero parallactic angle, and that the calibrator's position angle is  $45^\circ$ . These initial conditions should generate generally representative results for the 1 and 2 slice strategies, where the calibrator's Stokes



vector is known a priori and may therefore be targeted appropriately by observers. However, note that the initial conditions above (or any others) cannot fully represent all possible observing configurations for the 3 and 10 slice strategies, where the Stokes vector is unknown a priori. It is of course possible that rare specific configurations of these strategies could produce significantly different results than presented. It is worth noting here that when users in the linear feed basis are advised to maximize parallactic angle coverage, this really means they should maximise coverage for  $\mathcal{U}_\psi$  (i.e. maximum arc length traced along ellipse for a cross hand visibility). For a calibrator with unknown Stokes vector observed over as few as 3 slices, the difference in rare circumstances could be noticeable.

For the 1 slice strategy, the simulation code measures crosshand phase error by solving for a position angle in the noisy frame indicated by Equation 24 (i.e.  $\mathbf{Xf}$  solve in CASA terminology). For the 2 slice strategy, the code performs this step using the slice with maximum  $\mathcal{U}_\psi$  (known a priori). For the 3 and 10 slice strategies, the code measures crosshand phase error by solving for a linear slope with unconstrained offset, followed by a least squares fit to measure Stokes  $\mathcal{Q}$  and  $\mathcal{U}$  along this slope given the noisy observed variations of  $\mathcal{U}_\psi$  (i.e.  $\mathbf{XYf}+\mathbf{QUf}$  solve in CASA terminology).

For the multi-slice strategies, the code then performs a least squares fit to solve for two parameters in Equation A17: the observed  $d_{Xi}$  and  $\sum d_{Yj}^*$ . The latter is not needed for further analysis. The former is compared with the input value to compute the d-term error for the Monte Carlo sample under consideration, followed by conversion to spurious polarization using Equation A13. For the 1 slice strategy, the d-term error can be calculated more easily as the offset from the noisy measurement of the known Stokes vector.

## REFERENCES

- Conway, R. G., & Kronberg, P. P. 1969, MNRAS, 142, 11
- Cortes, P. C., Kameno, S., Nakanishi, K., et al. 2015, ALMA EOC Polarization Commissioning Report, ALMA Tech. Note (draft version Nov 23)
- Gardner, F. F., & Whiteoak, J. B. 1966, ARA&A, 4, 245
- Hales, C. A. 2017, Polarization calibration simulations presented in this work, v1.0, <http://dx.doi.org/10.5281/zenodo.801336>
- Hales, C. A. 2017, CASA Interferometric Pipeline Polarization Calibration & Imaging Requirement & Design Specifications, EVLA Memo Series, 201; also ALMA Memo Series, 603
- Hamaker, J. P., Bregman, J. D., & Sault, R. J. 1996, A&AS, 117, 137
- Martí-Vidal, I., Roy, A., Conway, J., & Zensus, A. J. 2016, A&A, 587, A143
- McMullin, J. P., Waters, B., Schiebel, D., Young, W., & Golap, K. 2007, Astronomical Data Analysis Software and Systems XVI, 376, 127
- Morris, D., Radhakrishnan, V., & Seielstad, G. A. 1964, ApJ, 139, 551
- Noordam, J. E. 1996, The Measurement Equation of a Generic Radio Telescope, AIPS++ Implementation Note, 185, [https://casa.nrao.edu/aips2\\_docs/notes/185/185.html](https://casa.nrao.edu/aips2_docs/notes/185/185.html)
- Price, D. C., & Smirnov, O. M. 2015, MNRAS, 449, 107
- Rayner, D. P., Norris, R. P., & Sault, R. J. 2000, MNRAS, 319, 484
- Sault, R. J., & Perley, R. A. 2013, Determining full EVLA polarization leakage terms at C and X bands, EVLA Memo Series, 170
- Sault, R. J., & Perley, R. A. 2014, Polarimetric calibration and dynamic range issues, EVLA Memo Series, 177
- Sault, R. J., Teuben, P. J., & Wright, M. C. H. 1995, Astronomical Data Analysis Software and Systems IV, 77, 433
- Sault, R. J., Hamaker, J. P., & Bregman, J. D. 1996, A&AS, 117, 149
- Smirnov, O. M. 2011, A&A, 527, A106